



Pancreatic cancer-targeting exosomes for enhancing immunotherapy and reprogramming tumor microenvironment

Wenxi Zhou^a, Yu Zhou^b, Xinli Chen^a, Tingting Ning^a, Hongyi Chen^a, Qin Guo^a, Yiwen Zhang^a, Peixin Liu^a, Yujie Zhang^a, Chao Li^a, Yongchao Chu^a, Tao Sun^a, Chen Jiang^{a,*}

^a Key Laboratory of Smart Drug Delivery, Ministry of Education, State Key Laboratory of Medical Neurobiology and MOE Frontiers Center for Brain Science, Department of Pharmaceutics, School of Pharmacy, Fudan University, Shanghai, 201203, China

^b Department of Interventional Radiology, Ruijin Hospital, Shanghai Jiao Tong University, School of Medicine, Shanghai, 200025, China

ARTICLE INFO

Keywords:

Pancreatic cancer immunotherapy
BM-MSC exosomes
Galectin 9/dectin 1 axis
Macrophage polarization
Immunogenic cell death

ABSTRACT

Immunotherapy has gained increasing focus in treating pancreatic ductal adenocarcinoma (PDAC), since conventional therapies like chemotherapy could not provide satisfactory improvement in overall survival outcome of PDAC patients. However, it is still not the game changing solution due to the unique tumor microenvironment and low cancer immunogenicity of PDAC. Thus, inducing more intratumoral effector immune cells as well as reversing immunosuppression is the core of PDAC treatment. Herein, we demonstrate an exosome-based dual delivery biosystem for enhancing PDAC immunotherapy as well as reversing tumor immunosuppression of M2-like tumor associated macrophages (M2-TAMs) upon disruption of galectin-9/dectin 1 axis. The deliver system is constructed from bone marrow mesenchymal stem cell (BM-MSC) exosomes, electroporation-loaded galectin-9 siRNA, and surficially modified with oxaliplatin (OXA) prodrug as an immunogenic cell death (ICD)-trigger. The use of biomaterials, BM-MSC exosomes, can significantly improve tumor targeting efficacy, thus increasing drug accumulation in the tumor site. The combined therapy (iEXO-OXA) elicits anti-tumor immunity through tumor-suppressive macrophage polarization, cytotoxic T lymphocytes recruitment and Tregs downregulation, and achieves significant therapeutic efficacy in cancer treatment.

1. Introduction

Pancreatic ductal adenocarcinoma (PDAC) is generally a fatal disease with a <6% five-year survival outcome [1]. Since limited benefits are demonstrated with traditional treatments like surgical resection and chemotherapy, new therapeutics for PDAC are under urgent demands. During recent years, immunotherapy is considered as a specific protective strategy for cancer treatment, which is characterized by activated host immune response, accompanied by recognition and elimination of tumor cells. Although immunotherapy has gained a tremendous momentum following the great success of immune checkpoint inhibitors in leukemia and melanoma, PDAC is disappointingly an exception due to its unique immunosuppressive tumor microenvironment (TME) and low cancer immunogenicity [2–4].

Other than tumor cells, the TME of PDAC is featured with exceedingly rich stroma, which almost takes 90% content of the tumor mass. Immune cells are not rare in the TME and comprise nearly 50% of the stroma cellular component, however, only a few of which are antitumor

effector cells [5]. In other word, most of the immune cells are hijacked immunosuppressive cells that are forced to facilitate the tumor progression. These suppressive leukocytes, including myeloid-derived suppressor cells (MDSCs), M2-polarized tumor associated macrophages (M2-TAMs), as well as regulatory T cells (Tregs), establish a comprehensive interaction, and inhibit the function of cytotoxic T lymphocytes through nutrition depletion, phenotype alternation, apoptosis and anergy [6,7]. In a recent preclinical study, a new mechanism was found between TAMs and tumor cells to exhibit an unexpected protumoral effect [8]. Galectin-9 (gal-9), a member of the β -galactoside-binding family of lectins, was found highly expressed in both mouse and human PDAC. The ligation of galectin-9 by dectin-1, a crucial innate immune receptor expressed on the surface of macrophages, can drive macrophages into protumoral M2 phenotype. Blockade of galectin-9 resulted in reversed immunosuppression, enhanced CD4⁺ and CD8⁺ T-cell effector activation and reduced tumor growth [6,8,9]. This suggests the potential of galectin-9 as a novel therapeutic target in immunotherapy of PDAC.

* Corresponding author.

E-mail address: jiangchen@shmu.edu.cn (C. Jiang).

<https://doi.org/10.1016/j.biomaterials.2020.120546>

Received 16 July 2020; Received in revised form 16 November 2020; Accepted 17 November 2020

Available online 23 November 2020

0142-9612/© 2020 Elsevier Ltd. All rights reserved.

However, even with increased understanding of the various mechanisms involved in PDAC progression, the special pathobiological barriers in PDAC TME, that is, the nearly-impenetrable-desmoplastic stroma with high solid stress, hypovascularity and hypoperfused tumor vessels, restricts the therapeutic response to many treatments, resulting a poor prognosis for patients [10,11]. Recent advances in biomaterials for drug delivery have been enabling significant progression in treating diseases, including major breakthroughs in PDAC, for example, liposomal irinotecan, reported to significantly improve median overall survival of PDAC patients in a clinical trial [12,13]. This showed the potential of biomaterial-based drug delivery strategies to be novel methods for fighting tumors. Though vesicle-like liposomes are promising to overcome the tough barriers and significantly increase drug accumulation in tumor tissues, regrettably, many of these synthetic delivery systems have poor stability and cause severe side effects, including systematic toxicity [14]. Hence, we investigate exosomes, a kind of natural derivative vehicles, as the drug deliver platform, which have unique advantages like nanosize, biodegradable features and tumor-homing function in PDAC treatment [15]. Exosomes (40–150 nm diameters) are cell-derived membrane vesicles with a lipid bilayer structure which function as a cell-to-cell communicator, and also capable to deliver chemotherapeutics, proteins or genes against tumor [15–17]. Remarkably, exosomes also show improved stability, enhanced endocytosis and reduced toxicity *in vivo* [15]. In our previous study, exosomes derived from bone marrow mesenchymal stem cells (BM-MSCs) have showed the tumor homing function in PDAC mouse models [18]. These evidences demonstrate that exosomes can serve as an attractive nanoscale drug delivery platform for pancreatic cancers.

Another obstacle in PDAC immunotherapy is the low immunity, which means patients bearing pancreatic tumor get rare intratumoral effector T cells [19]. Since the antitumor effect of immunotherapy largely depends on the tumor infiltration of cytotoxic T lymphocytes, there exists an urgent need to boost the immune response and recruit more tumor killing immune cells in PDAC. Recently, researches show that inducing immunogenic cell death (ICD) of tumor cells is a promising strategy to elicit antitumor immunogenicity in support of immunotherapy [20]. Preclinical reports have suggested that some chemotherapeutics are capable of inducing ICD responses [21]. Upon treatment with these agents, apoptotic tumor cells express calreticulin (CRT) on the surface, subsequently release high mobility group box 1 (HMGB1) and secrete adenosine triphosphate (ATP). CRT plays a role as the “eat me” signal to elicit phagocytosis of dying tumor cells by dendritic cells

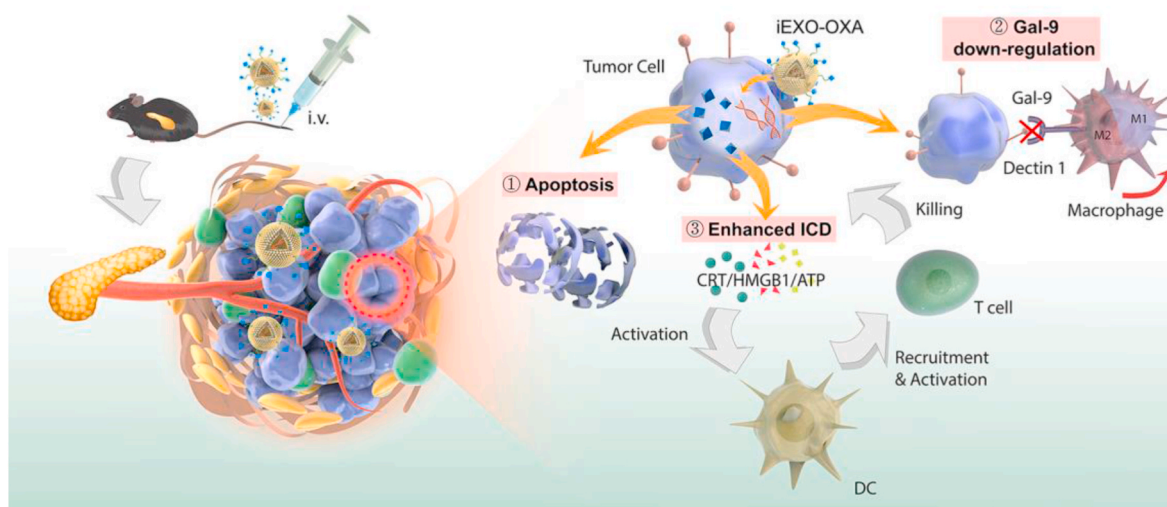
(DCs), while HMGB1 and ATP act as immunostimulatory signals to initiate DCs maturation and antigen presentation, which further activate the antitumor immune response and promote infiltration of cytotoxic T lymphocytes (CTLs) in TME [22–24]. Therefore, chemotherapy-induced ICD may offer a promising strategy to trigger the dormant innate and/or adaptive immune response and kill tumor cells.

Inspired by the above work, a PDAC-targeting exosome-based bio-platform was designed for enhancing immunotherapy and reprogramming TME (Scheme 1). Oxaliplatin (OXA), a component of FOLFIRINOX regimen used in PDAC, was applied to both trigger ICD effect in pancreas tumor site and kill the tumor cells by inhibiting DNA synthesis and repair [25]. To further increase the antitumor effect, gal-9 siRNA treatment was combined to block galectin-9/dectin-1 axis to reverse immunosuppression caused by M2-TAMs. In achieving the combined therapy, exosomes were applied as the carriers of both OXA and siRNA, which were also beneficial to improve the drug delivery efficiency, tumor homing and duration of action. After the preparation of siRNA-EXO-OXA (iEXO-OXA) nanoparticles, *in vitro* and *in vivo* experiments demonstrated that iEXO-OXA can be preferentially delivered to tumor site, protect the cargo gene, elicit anti-tumor immunity, enhance blood circulating time, and offer significant therapeutic effect to treat established PANC-02 tumors.

2. Materials and methods

2.1. Materials and reagents

Oxaliplatin was purchased from Meilunbio (Dalian, China). Succinic anhydride and *N*-(2-Aminoethyl) maleimide trifluoroacetate salt were purchased from Aladdin Chemistry (Shanghai, China). 0.22 μ m syringe filters were purchased from Meck-Millipore (Billerica, MA, USA). Opti-Prep™ Density Gradient Medium (iodixanol-based solution) was purchased from Sigma-Aldrich (Billerica, MA, USA). 3-(4,5-dimethyl-2-thiazolyl)-2,5-diphenyl- β H tetrazolium bromide (MTT) and 4',6-diamidino-2-phenylindole (DAPI) were purchased from Sigma-Aldrich (St. Louis, USA). Annexin V-FITC/PI apoptosis detection kit and Cell Cycle Detection Kit were purchased from KeyGEN BioTECH (Nanjing, China). Bodipy, Exosome Spin Columns (Mw 3000), IL-10 and IFN- γ ELISA kit were purchased from ThermoFisher (Waltham, MA, USA). Prime-Script™ RT reagent Kit (Perfect Real Time, RR037A) and TB Green Premix Ex Taq™ (Tli RnaseH Plus, RR420A) were purchased from TaKaRa (Beijing, China). All the antibodies were purchased from Abcam



Scheme 1. Pancreatic cancer-targeting exosomes for enhancing immunotherapy and reprogramming tumor microenvironment: 1) Tumor cell apoptosis caused by chemotherapeutic agent oxaliplatin; 2) Galectin-9 down-regulation by siRNA treatment to achieve macrophage polarization; 3) Oxaliplatin-triggered ICD response with CRT exposure on dying tumor cell surfaces and release of HMGB1 and ATP to activate DC maturation.

(Shanghai, China). All the other reagents were purchased from Sino-pharm Chemical Reagent (Shanghai, China).

2.2. Cell lines

BM-MSC cells, purchased from ScienCell (San Diego, CA, USA), were carefully expanded and maintained in Mesenchymal Stem Cell Medium (ScienCell, San Diego, CA, USA) supplemented with 10% exosome-free fetal bovine serum (FBS) (Gibco, Carlsbad, CA, USA) and 1% Penicillin-Streptomycin solution. PANC-02 cells, a kind gift from Prof. Zhigang Zhang at Shanghai Cancer Institute, were carefully expanded and maintained in high glucose DMEM medium (Sigma-Aldrich) supplemented with 10% heat-inactivated FBS and 1% Penicillin-Streptomycin solution. All the cells were incubated under a saturating humidity atmosphere at 37 °C containing 5% CO₂.

2.3. Animals

C57BL/6 mice (male, 18–20 g) were purchased from Slac Laboratory Animal Co. Ltd. (Shanghai, China) and carefully maintained under standard laboratory conditions. Orthotopic PANC-02 pancreatic tumor models were established by injecting 1.0×10^6 PANC-02/luci cells in 100 µL Hank's buffer at pancreas of male C57BL/6 mice. The mice were administered with 100 µL D-luciferin potassium solution (30 mg/mL) by intraperitoneal injection and detected 20 min later by IVIS Spectrum (PerkinElmer Inc., Waltham, MA, USA) to monitor the growth of tumor. All the animal experiments were under strict guidelines evaluated and approved by Institutional Animal Care and Use Committee (Fudan University).

2.4. Isolation, purification and characterization of exosomes

The exosomes were isolated from the supernatant of BM-MSCs, followed by differential centrifugation processes and sucrose gradient separation, as previously reported [26]. Exosome-free FBS was prepared by ultracentrifugation (CP100NX, HITACHI) at 120,000 g for 16 h and filtration with 0.22 µm syringe filters. After incubation with BM-MSC medium containing exosome-free FBS for 48 h, supernatant from cells was collected and isolated with sequential centrifugation steps as follows: centrifugated at 800 g for 5 min to remove the dead cells, at 1500 g for 15 min to remove the cellular debris and at 15,000 g for 30 min to remove the large extracellular vesicles. The resulting supernatant was subsequently ultracentrifugated at 150,000 g for 2 h. The purified exosomes were then characterized and used for experiments.

For further exosome purification, iodixanol-sucrose density gradient was performed as shown in Scheme S2. For the bottom-up iodixanol-sucrose gradient separation, a 11.5 mL discontinuous iodixanol-sucrose gradient (40%–5% iodixanol solution, 0.25 mM sucrose, pH 7.4) was built into a 12 mL ultracentrifugation tube. Purified exosomes resuspended in 500 µL PBS 7.4 were added to the top of the gradient and then ultracentrifugated at 120,000 g for 16 h. Gradient solution was separated into 12 tubes with 1 mL liquid per tube from the top to bottom and density of each was assessed by a refractometer. As the density of exosomes range from 1.13 to 1.19 g/mL, liquid in No.6 and No.7 tubes was collected and added with PBS to a final volume of 20 mL. Then the solution was ultracentrifuged at 150,000 g for 2 h. The pellets on the bottom were resuspended in 500 µL PBS and could be stored at –80 °C. All the centrifugation was performed at 4 °C.

For the detection of concentration and hydrated diameters of exosomes, 100 µL exosome was diluted into 1 mL and analyzed by NTA (NanoSight NS300, Malvern Panalytical, Malvern, UK). Approximately $\sim 10^8$ exosomes were collected and weighted 0.5–1 mg after freeze-dried. The morphology of exosomes was observed under TEM (Tecnaei G2 spirit Biotwin, FEI). Annexin V, CD63, Alix, Hsp70, CD81 and β-actin were verified by Western blotting as the biomarkers of exosomes. To check the exosomes *in vitro* or *in vivo*, Bodipy 650/665 was modified to

the outside membrane of exosomes. Briefly, 5 µL 1 mg/mL Bodipy solution was added to 10^8 exosomes in 500 µL PBS 7.4 and vortexed for 0.5 h. Unbounded Bodipy probe was removed by Exosome Spin Columns according to the protocol.

2.5. Preparation and characterization of iEXO-OXA

To load galectin-9 siRNA, electroporation was applied using a Gene Pulser X Cell Electroporation System according to the protocol. $\sim 10^9$ exosomes (measured by NTA) were mixed with 1.5 µg siRNA in 400 µL electroporation buffer (1.15 mM potassium phosphate pH 7.2, 25 mM potassium chloride, 21% Optiprep), electroporated with 400 V, 125 µF and $\infty \Omega$ and immediately transferred onto ice afterwards. Then the electroporation buffer was replaced with 2 mL PBS 7.4 by ultracentrifugation as previously described, preparing for the loading of oxaliplatin. 2 mg OXA-MAL was added to the exosomes and obtained stable maleimide-thiol conjugates *via* vortexing according to the reports [27]. Unbounded oxaliplatin prodrugs were removed by Exosome Spin Columns (Mw 3000) (ThermoFisher, Waltham, MA, USA). Sizes and concentration of the freshly prepared nanoparticles were measured by NTA. The morphology of the formulation was observed under TEM.

To measure the amount of gal-9 siRNA electroporated into exosomes, Cy5-tagged siRNA was used and fluorescent signal was evaluated by a Multiskan MK3 microplate reader (Thermo Scientific, Waltham, Massachusetts, USA). The siRNA quantification was also performed using PrimeScript™ RT reagent Kit and TB Green Premix Ex Taq™ by QuantStudio 3 Real-Time PCR System. The amount of oxaliplatin loaded onto exosomes was measured by HPLC (Agilent 1220, Agilent, Santa Clara, CA, USA). 500 µL iEXO-OXA solution was freeze-dried to measure the weight and then incubated with PBS 7.4, 2 mM Vit C in a shaking bath at 100 rpm, 37 °C for 1 h. The external medium was collected and measured by HPLC method at a flow rate of 1 mL/min by UV detector at 250 nm (95% CH₃OH, 5% H₂O).

2.6. Cellular uptake studies of exosomes

PANC-02 cells were seeded in a 6-well plate (Corning-Coaster, Tokyo, Japan) with a density of 1.0×10^5 cells/well. When monitored a confluency of 80–90%, cells were incubated with Bodipy-labeled exosomes in DMEM medium at 37 °C for 1, 2, 4 and 6 h, respectively. After wash with Hank's for 3 times, cells were visualized by Confocal Laser Scanning Microscope (CLSM, Carl Zeiss LSM710, Carl Zeiss, Jena, Germany). Quantitative assay of cellular uptake was also performed by flow cytometer (FACS, BD Biosciences, Bedford, MA).

2.7. Biodistribution study of exosomes *in vivo* and *ex vivo*

In vivo biodistribution study was carried out on orthotopic PANC-02/luci tumor-bearing mice (n = 3). Ten-day post implantation with PANC-02 cells, mice were intravenously injected with free Bodipy and Bodipy-labeled exosomes. *In vivo* fluorescent signals of exosomes were observed at indicated time points by Xenogen IVIS Spectrum. For liver function test, 48 h post injection, blood samples (0.5 mL) were collected into heparinized tubes and centrifuged at 4000 rpm for 10 min. The supernatant was collected from each tube and liver enzyme levels (ALT, alanine aminotransferase; AST, aspartate aminotransferase) were tested by Wuhan servicebio technology CO.,LTD. Then mice were sacrificed. Major organs and the whole tumor tissues were harvested and measured by IVIS spectrum. For the tumor section observation, tumor tissues were fixed with 4% paraformaldehyde, dehydrated with sucrose solutions, embedded with OCT medium and then cut into slides. The sections were stained with anti-collagen 1 (anti-COL-1) (ab6308) and anti-α-smooth muscle actin (anti-α-SMA) (ab32575) antibodies to visualize extracellular matrix and fibroblasts, respectively. After stained with DAPI, the frozen slices were photographed by CLSM.

2.8. Stability of iEXO-OXA *in vitro* and *in vivo*

For *in vitro* study, iEXO-OXA was suspended in PBS and isotonic sucrose, size of which was tested every day by NTA during a 7-day observation period. For *in vivo* study, Bodipy-labeled iEXO-OXA (Bodipy-iEXO-OXA), Bodipy-labeled exosomes (Bodipy-EXO), free Bodipy, iEXO-OXA and free OXA (OXA 5 mg/kg, $\sim 10^9$ exosomes per rat equiv.) were injected into healthy male SD rats *via* tail vein, respectively ($n = 3$). At 1, 4, 8, 12, 24 and 48 h, blood samples (0.5 mL) were collected into heparinized tubes. For the determination of fluorescence of Bodipy, each sample was taken 100 μ L of the whole blood and tested under a microplate reader. For the determination of the concentration of Pt, 200 μ L of each sample was tested by ICP-MS.

2.9. Evaluation of galectin-9 gene silencing of iEXO

The expression of galectin-9 at mRNA level in normal cell line (HEK 293, as control) and pancreatic cancer cell lines (PANC-02, MIAPaCa-2) were detected by semi-quantitative q-PCR. For *in vitro* transfection, exosomes were electroporated with galectin-9 siRNA as described above. PANC-02 cells were seeded in a 6-well plate with a density of 1.0×10^5 cells/well and treated with exosomes. Cells treated with Lipo6000™ transfection reagent (Beyotime Biotechnology, Shanghai, China) were set as the positive control. After 48 h-incubation, total RNA of cells in different groups was extracted, reverse transcribed and tested by three times to define a biological replicate. Primer sequences were as follows: galectin-9: forward 5'-GACAGATGTTCTCTACTCCCGC-3', reverse 5'-TGACAGGAGGATGGACTTGGAT-3'; actin: forward 5'-CACCCAGCACAATGAAGATCAAGAT-3', reverse 5'-CCAGTTTT-TAAATCTGAGTCAAGC-3'.

For western blotting, PANC-02 cells were treated as described above. After 48 h-incubation, cells were washed with PBS thrice and lysed with RIPA lysis buffer according to the protocol. The protein concentration of the resulting cell lysis was measured by BCA protein assay (Beyotime Biotechnology, Shanghai, China). Totally 25 μ g proteins of each samples were separated by 10% SDS-PAGE and transferred onto PVDF membranes (Mini-PEOTAN, Bio-Rad). Subsequently, membranes were blocked with 5% nonfat milk for 1 h at room temperature and incubated with anti-galectin-9 (ab69630) and anti-GAPDH (Beyotime, AF0006) primary antibodies at 4 °C overnight. HRP-conjugated secondary antibodies were then incubated for 2 h at room temperature, followed with detection by chemiluminescent reagents, and membranes were visualized by Image Lab (Bio-Rad).

2.10. Investigation of macrophage polarization *in vitro*

Fresh mouse peritoneal macrophages were harvested as previously reported [28]. The extracted macrophages were seeded in a 6-well plates with a density of 1.0×10^5 cells/well. When achieving 70–80% confluence, macrophages were cocultured with IL-4 (20 ng/mL), PANC-02 cells and PANC-02 cells pretreated with iEXO, respectively. After 12 h incubation, macrophages were washed with Hank's thrice and harvested into tubes, respectively. Cells were block with BSA for 15 min, subsequently incubated with anti-F4/80-FITC, anti-CD16/32-PE, anti-CD206-PE-Cyanine 7 antibodies and then analyzed by FACS.

2.11. Antitumor efficacy *in vitro*

Antitumor efficacy of Platinum-based formulations *in vitro* was tested by MTT assay and Annexin-V/PI assay. For MTT assay, PANC-02 cells were seeded in 96-well plates at a density of 2.0×10^3 cells/well. After incubated overnight, cells were treated with exosomes, oxaliplatin, EXO-OXA or iEXO-OXA at an oxaliplatin concentration range from 1 nM to 400 μ M. After another 48 h incubation, the supernatant was removed and cells were washed with Hank's thrice before treated with 100 μ L 0.5 mg/mL MTT solution. 4 h later, the supernatant was removed and the

residuals were incubated with 100 μ L DMSO for 10 min to dissolve the formazan crystal. The absorbance of formazan was measured at 570 nm by a microplate reader. For *in vitro* apoptosis assay, Annexin-V/PI assay was applied. In brief, PANC-02 cells were seeded in a 6-well plate with a density of 1.0×10^5 cells/well and cultured overnight. The cells were then treated with exosomes, oxaliplatin, EXO-OXA or iEXO-OXA at an equivalent oxaliplatin concentration of 20 μ M for 48 h. Afterwards, cells were harvested into tubes, respectively, washed with Hank's thrice, resuspended with binding buffer and incubated with Annexin-V/PI according to the protocol. Apoptotic cells were evaluated by FACS and visualized by fluorescence microscope (Leica, Wetzlar, Germany).

2.12. Cell cycle analysis

PANC-02 cells were seeded in a 6-well plate with a density of 1.0×10^5 cells/well and cultured overnight. After incubation with FBS-free medium for another 12 h, cells were treated with exosomes, oxaliplatin, EXO-OXA or iEXO-OXA at an equivalent oxaliplatin concentration of 10 μ M for 24 h. Subsequently, cells were harvested into tubes, respectively, fixed with 70% cold ethanol for 2 h and stained with PI/RNase A solution according to the protocol (KeyGEN DNA content Quantitation Assay Kit). The population of PANC-02 cells at different cell cycle stages was quantified by FACS and analyzed by ModFitLT V3.2 software.

2.13. Induction of immunologic cell death (ICD) *in vitro*

PANC-02 cells were seeded in a 6-well plate with a density of 1.0×10^5 cells/well and cultured overnight. Cells were treated with exosomes, oxaliplatin, EXO-OXA or iEXO-OXA at an equivalent oxaliplatin concentration of 50 μ M for 4 h. Subsequently, cells were washed with cold Hank's thrice and stained with anti-CRT (ab22683) and anti-HMGB1 (ab79823) primary antibodies at 4 °C overnight, respectively, followed by secondary antibodies Goat anti-rabbit IgG Alexa Fluor 488 and Goat anti-mouse IgG Alexa Fluor 488. After stained with DAPI, fluorescent signals of CRT and intracellular HMGB1 were visualized by CLSM. For HMGB1 release assay, the supernatant of the culture medium above was centrifugated to remove the dead cells and ultrafiltrated into 100 μ L. Released HMGB1 was detected *via* western blotting.

2.14. Antitumor efficacy *in vivo*

According to the bioluminescence signal of tumors detected by IVIS spectrum, 56 male C57BL/6 mice bearing orthotopic PANC-02/luci tumor were randomly divided into seven groups ($n = 8$). Mice were intravenously injected with PBS, GEM, OXA, Scrbl-iEXO, iEXO, EXO-OXA and iEXO-OXA (with an equivalent oxaliplatin concentration of 5 mg/kg and $\sim 10^8$ exosomes) every 3 days for 5 times. Body weight was recorded every other day and bioluminescence signal of tumors were monitored by IVIS spectrum.

2.15. Western blotting *in vivo*

Tumor tissue samples were collected after a course of different treatments and lysed with RIPA lysis buffer according to the protocol. The protein concentration was measured by BCA protein assay. Totally 25 μ g proteins of each samples were separated by 10% SDS-PAGE and transferred onto PVDF membranes. Subsequently, membranes were blocked with 5% nonfat milk and incubated with anti-galectin-9, anti-HMGB1 and anti- β -actin (Beyotime, AA128-1) primary antibodies. HRP-conjugated secondary antibodies were then incubated for 2 h, followed with detection by chemiluminescent reagents, and membranes were visualized by Image Lab.

2.16. Flow cytometric analysis of immune cells population

Tumor draining lymph nodes and tumor tissue samples were

collected after a course of different treatments and cut into small pieces, followed with dispersion into single cells. Prepared samples were then blocked with BSA for 20 min and afterwards, stained with anti-CD11c-FITC, anti-CD80-APC, anti-CD86-PE, anti-CD45-APC, anti-CD11b-APC-eFluor 780, anti-CD16/32-PE, anti-CD206-PE-Cyanine 7, anti-CD4-PerCP-Cyanine 5.5, anti-CD8-PE, anti-CD25-PE-Cyanine 5, anti-FoxP3-eFluor 450 antibodies. Mature DCs (CD11c⁺CD80⁺CD86⁺), M1-TAM (CD45⁺CD11b⁺CD16/32⁺), M2-TAM (CD45⁺CD11b⁺CD206⁺), CTL cells (CD45⁺CD4⁺CD8⁺), helper T cells (CD45⁺CD4⁺CD8⁻) and Tregs (CD45⁺CD4⁺CD25⁺FoxP3⁺) were evaluated by FACS, respectively.

2.17. Immunofluorescence staining

For the tumor section observation, tumor tissues were harvested and cut into slides as described above. The sections were stained with anti-CD16/32-PE, anti-CD206-PE-Cyanine 7, anti-F4/80-FITC, anti-CD4-PerCP-Cyanine 5.5, anti-CD8-PE, anti-FoxP3-eFluor 450, anti-galectin-9, anti-COL-1 antibodies, respectively. After stained with DAPI, the frozen slices were photographed by CLSM.

2.18. Measurement of tumor cytokines

Tumor tissue samples were prepared as described above. IL-10 and IFN- γ was valued by Mouse IL-10 ELISA kit and Mouse IFN- γ ELISA kit according to the protocol.

2.19. H&E staining

For safety evaluation, the main organs (heart, liver, spleen, lung, and kidney) were harvested and fixed with 4% paraformaldehyde, dehydrated with sucrose solutions, embedded with paraffin and then cut into slides. The sections were then stained with hematoxylin and eosin. Afterwards, stained tumor slices were photographed by the inverted fluorescent microscope.

2.20. Statistical analysis

All the data were analyzed by GraphPad Prism 7.0 software and presented as means \pm standard deviation (SD), and comparison between groups was performed by one-way ANOVA. Statistical significance was defined as *P < 0.05, **P < 0.01, ***P < 0.001, ****P < 0.0001.

3. Results and discussion

3.1. Preparation and characterization of iEXO-OXA

The experimental steps to prepare the dual delivery biosystem was outlined in Fig. 1a and Scheme S1. Firstly, exosomes were isolated from the supernatant of BM-MSCs culture medium by differential centrifugation processes (Scheme S2) [18]. Galectin-9 siRNA was electroporated into exosomes according to the protocol [29,30]. As for delivering OXA, a prodrug form (OXA-MAL) was synthesized by oxidizing oxaliplatin to OXA(IV)-OH, followed by modification with *N*-(2-Aminoethyl) malimide. The successful synthesis of OXA-MAL was characterized by ¹H NMR (Fig. S1). Subsequently, EXO-siRNA (designated as iEXO) was modified with OXA-MAL via vortex to prepare iEXO-OXA. Nanoparticles tracking analysis (NTA) demonstrated empty exosomes and iEXO-OXA with an average diameter of 122 \pm 35.3 nm and 140 \pm 37.6 nm, respectively (Fig. 1b and e). The morphology shown by transmission electron microscopy (TEM) displayed natural bowl shape appearances of the exosomes with a low background, suggesting the high purity of the samples (Fig. 1c and f; Fig. S2). The similar results between exosomes and iEXO-OXA indicated that the electroporation and modification with chemotherapeutic prodrugs didn't significantly change the physico-chemical property of the formulations. Besides, Annexin V, CD63, Alix, Hsp70 and CD81 were verified by western blotting as the biomarkers of exosomes (Fig. 1d). The loading capacity of siRNA in 10⁹ exosomes was 0.5678 \pm 0.0258 μ g (Fig. S3). And the encapsulation efficiency and loading capacity of OXA in iEXO-OXA were measured by HPLC to be 13.17% and 5.71 w/w%, respectively (Fig. S4 and 5).

3.2. Enhanced cellular uptake efficiency and improved primary PDAC tumor-targeting ability of BM-MSC exosomes

In order to initiate the apoptosis of tumor cells, efficient cellular uptake was required. And the investigation of cellular uptake of exosomes was carried out in PANC-02 cells. Tumor cells were cultured with Bodipy-labeled exosomes and incubated for indicated time, after which cells were monitored under microscopy or tested by FACS (Fig. S6). Internalization of Bodipy-exosomes by PANC-02 cells was time-dependent and the saturation was around 6 h. Hypothesis for exosome internalization have been reported in literature, including vesicle-cell fusion, endocytosis, macropinocytosis and phagocytosis [31–33].

Based on the *in vitro* uptake results, we further examined the tumor-targeting ability of exosomes *in vivo* in PANC-02 tumor-bearing mice.

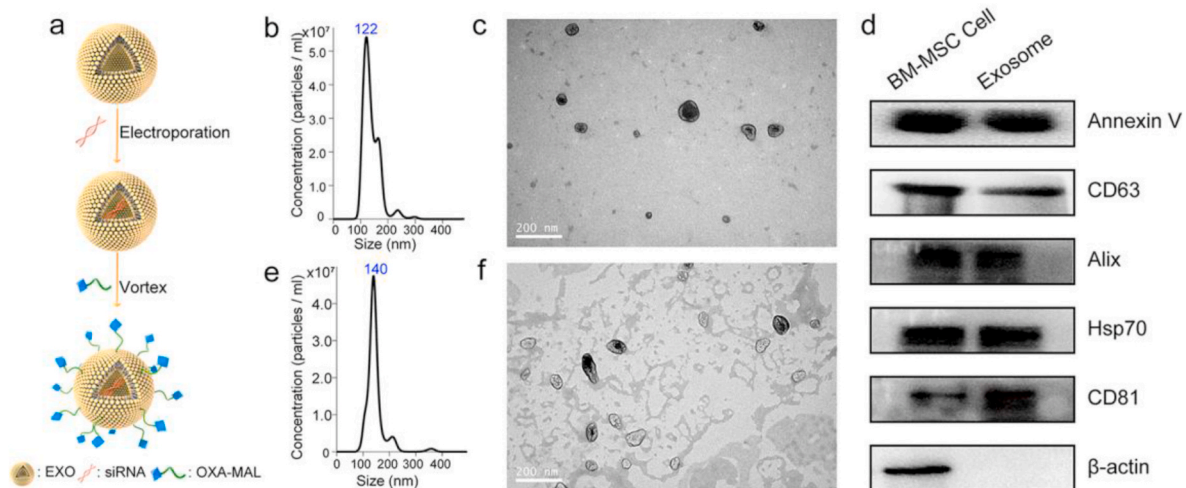


Fig. 1. Characterization of iEXO-OXA. a) Scheme of preparation of iEXO-OXA. b) NTA results of diameter and concentration of exosomes. c) Representative images of the morphology of exosomes observed with TEM (scale bar: 200 nm). d) Biomarkers of exosomes by western blotting. e) NTA results of diameter and concentration of iEXO-OXA. f) Representative images of the morphology of iEXO-OXA observed with TEM (scale bar: 200 nm).

After tail-vein injection with Bodipy-iEXO-OXA, Bodipy-EXO and free bodipy (as control), three groups of mice were observed at indicated time points (0, 4, 12, 24, and 48 h) by IVIS system (Fig. 2a and Fig. S7). Notably, near-infrared (NIR) signal was continuously accumulated in the tumor site of group Bodipy-iEXO-OXA and group Bodipy-EXO, but systematically distributed in control group as time lapsed, which proved that exosomes had specific PDAC tumor-targeting ability and relatively prolonged circulation time. The whole tumor tissue and other major organs (heart, liver, spleen, lung, and kidney) were harvested, showing similar biodistribution tendencies (Fig. 2b and c). Furthermore, frozen tumor sections were stained with COL-1 and α -SMA antibodies (green), representing extracellular matrix and fibroblasts, respectively. As showed in Fig. 2d–g, Bodipy-iEXO-OXA and Bodipy-EXO (red) could be detected in the deep site of the tumor even though the stroma was dense, indicating the penetrating capability of exosomes. Moreover, the stability of iEXO-OXA was determined both *in vitro* and *in vivo*. For *in vitro* study, iEXO-OXA was suspended in PBS and isotonic sucrose, and they exhibited no obvious increase in size during a 7-day observation period (Fig. S8 a, b). For *in vivo* study, we determined the whole blood clearance

of exosomes and iEXO-OXA. As shown in Fig. S8c and d, Bodipy-labeled iEXO-OXA had lower clearance than free Bodipy, and iEXO-OXA had lower Pt clearance than OXA, indicating the prolonged circulation time of the conjugation. Besides, no liver toxicity was found, showing the biosafety of our formulations (Fig. S9).

Studies showed that BM-MSCs derived exosomes could home to pancreatic cancer efficiently *in vivo* due to the intimate interaction between BM-MSCs and PDAC tumor tissue, instead of being mostly distributed to the liver and spleen in healthy mice [18,34–36]. Meanwhile, some membrane-anchored proteins of exosomes could also amplify the homing effect and penetrating capability [8]. Compared with parent MSCs, increasing evidence showed that BM MSC-derived exosomes might provide a new cell-free therapy with advantages such as lower immunogenicity and decreased risk of tumor progression [37].

Thus, based on the above features, exosomes could enhance cellular uptake efficiency, improve primary PDAC tumor-targeting ability, and satisfy the essential requirements for anti-tumor drug carriers.

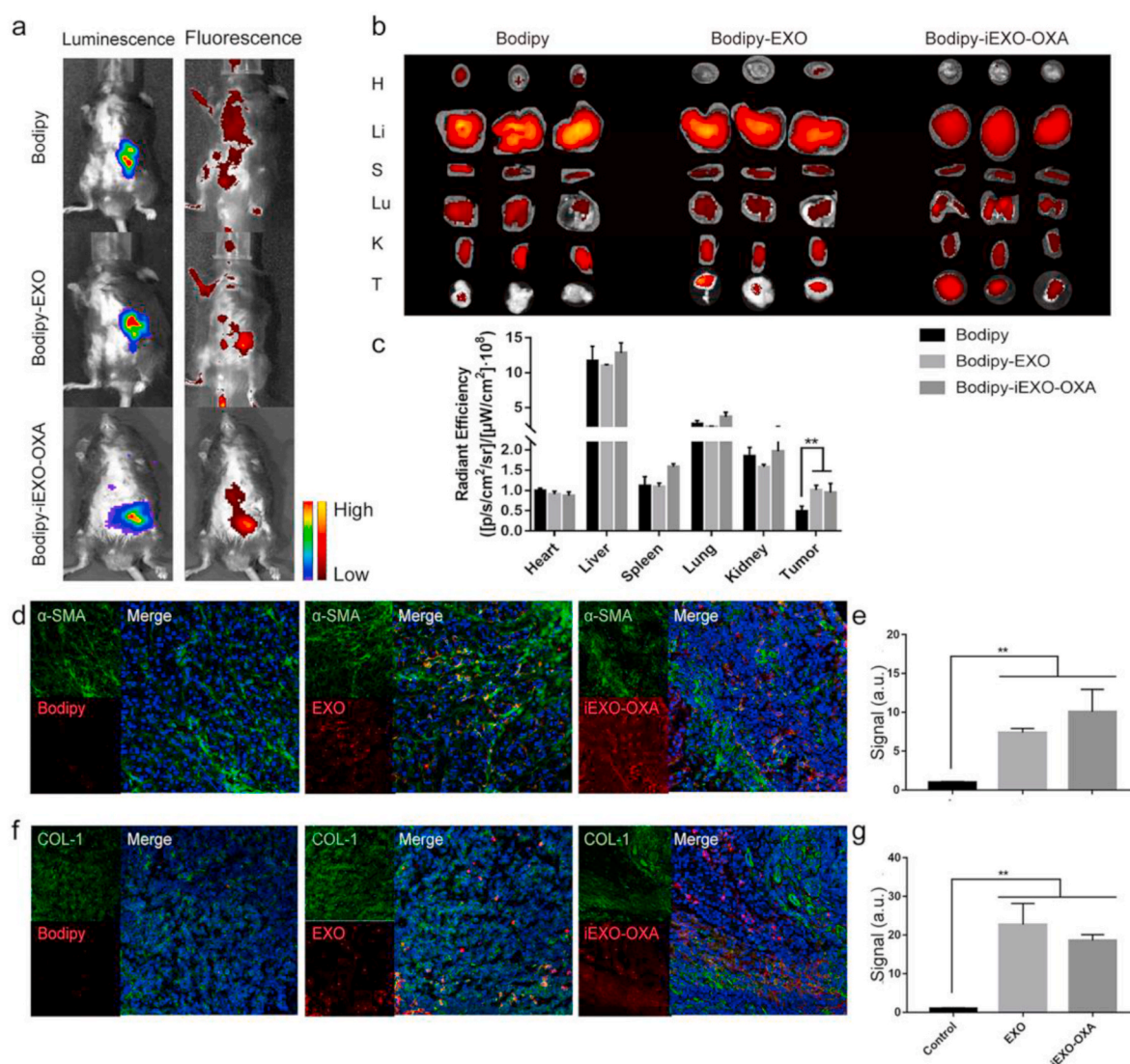


Fig. 2. *In vivo* targeting effect of iEXO-OXA. a) *In vivo* IVIS imaging of mice after tail-vein injection with Bodipy, Bodipy-EXO or Bodipy-iEXO-OXA after 24 h (n = 3, 5 mg OXA/kg, $\sim 10^8$ exosomes per mouse). b) *Ex vivo* IVIS images of major organs and tumor tissues from PANC-02 mice models 48 h after treatment with different formulations (n = 3). c) Quantification of the fluorescence intensity by measuring region of interest (ROI) in (b) (n = 3). d) and f) Tumor tissue immunofluorescent images under LCSM. (blue: DAPI for nucleus; green: Alexa Fluor 488 labeled α -SMA or COL-1; red: Bodipy, Bodipy-EXO or Bodipy-iEXO-OXA; original magnification = 200). e) and g) Statistical results of the Bodipy signals of different groups (n = 3). Data presented as mean \pm SD, one-way ANOVA, ***p* < 0.01.

3.3. Downregulation efficacy of Galectin-9 siRNA treatment and macrophage polarization assay *in vitro*

We first verify the downregulation effect of gal-9 siRNA treatment *in vitro*. PANC-02 cells were incubated with iEXO for 6 h, setting iLIPO (Lipo6000™-based gal-9 siRNA transfection strategy) as a positive control. Both qPCR and western blotting showed relevant results, where iEXO could significantly reduce mRNA and protein levels of galectin-9 in mouse PANC-02 cells, with superior efficacy compared to iLIPO (Fig. 3a and b). To further assess the function of iEXO in macrophage polarization *in vitro*, fresh collected mouse peritoneal macrophages were co-incubated with IL-4, PANC-02 cells and PANC-02 cells pretreated with iEXO (group PANC-02@iEXO), respectively. Results from flow cytometric analysis illustrated a significant reduction of M2-like macrophages in group iEXO (Fig. 3c and d), indicating the efficacy of iEXO in driving macrophages to antitumor phenotype. Taken together, iEXO could effectively downregulate the target gene in PANC-02 cells, thus interrupting the connection between tumor cells and macrophages to prevent macrophage polarization *in vitro*.

3.4. Enhanced cytotoxicity and ICD response of iEXO-OXA on PANC-02 cells

Subsequently, an MTT assay was conducted to demonstrate the cytotoxic effect of OXA-based formulations. Upon incubation with OXA,

EXO-OXA and iEXO-OXA, significant cell viability inhibition was observed (Fig. 3e). The antitumor efficacy was further investigated by Annexin-V/PI assay, where Annexin-V signal represented the early apoptosis and PI signal indicated cells in late apoptosis. Images from the microscopy showed that the fluorescent intensity was significantly higher in group EXO-OXA and iEXO-OXA than the others (Fig. 3j). For the quantitative analysis, the cells were then collected, resuspended, and analyzed by FACS (Fig. 3f and g). Compared with group OXA (3.61%), enhanced cytotoxicity was observed in group EXO-OXA and iEXO-OXA (9.92% and 13.8%, respectively). Meanwhile, since OXA affected on cell cycle progression by blocking DNA synthesis, cell cycle arrest experiment was examined and we confirmed that the exosome-based bio-platform still possessed the capability of cell cycle inhibition (Fig. S11).

ICD is a cell death modality that can be used to stimulate an effective immune response against tumors with the changes in the composition of cell surfaces (CRT exposure) as well as the release of soluble mediators (for example, HMGB1) [38]. Since OXA-based drugs could trigger ICD in tumor cells, CRT exposure was then monitored on the surface of PANC-02 cells under microscopy after short-term stimulation with different formulations, followed by flow cytometric analysis. As illustrated in Fig. 3k and Fig. S12, the largest number of CRT staining cells were detected in group EXO-OXA and iEXO-OXA, indicating the enhanced ICD-associated immunogenicity in these two groups. Besides, higher release of HMGB1 from the nuclei to cytosol, was also detected via fluorescence microscopy after treatments with EXO-OXA and

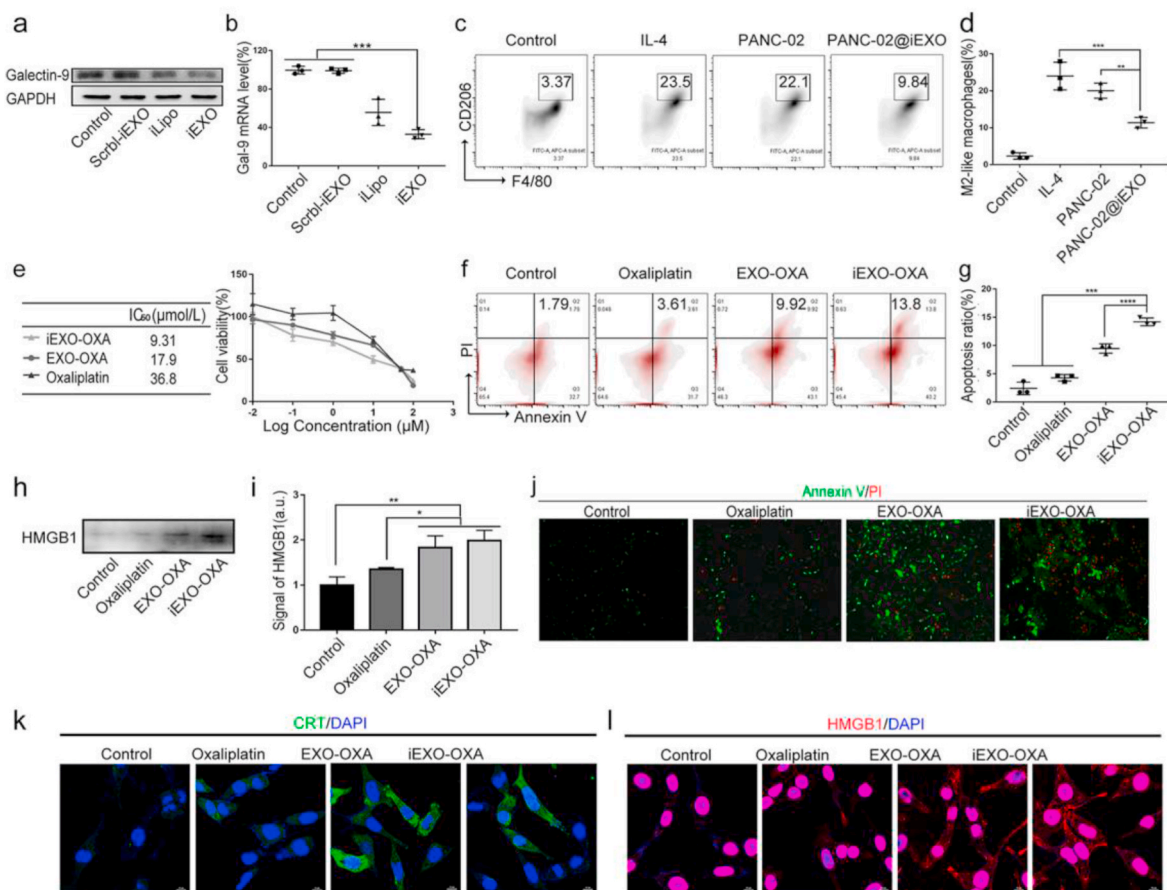


Fig. 3. *In vitro* study of iEXO-OXA. Down regulation of galectin-9 in PANC-02 cells with different treatment by a) western blot and b) RT-PCR (n = 3). c) Primary mice peritoneal macrophage polarization after treatment with different formulations by FACS. d) Statistical results of c) (n = 3). e) Proliferative inhibition and IC₅₀ of different formulations (n = 4). f) Flow cytometry analysis of cell apoptosis gating on Annexin V-FITC/PI staining. g) Statistical results of f) (n = 3). h) HMGB1 secretion in the supernatant of PANC-02 cells after treatment with different formulations by western blotting. i) Statistical results of h) (n = 3). j) Annexin-V/PI assay of cell apoptosis by fluorescence microscope. (green: annexin-V; red: PI; original magnification = 200). k) CRT exposure and l) HMGB1 secretion in PANC-02 cells after treatment with different formulations by CLSM (scale bar: 10 μm). Data presented as mean ± SD, one-way ANOVA, **p* < 0.05, ***p* < 0.01, ****p* < 0.001, *****p* < 0.0001.

iEXO-OXA (Fig. 3l). Additionally, increased secretion of HMGB1 from PANC-02 cells into extracellular medium was detected in these two groups *via* western blotting (Fig. 3h and i). Altogether, the exosome-based OXA-delivery system could improve cytotoxicity of the chemotherapy agent and enhance ICD response *in vitro*.

3.5. *In vivo* antitumor efficacy and enhanced immunity of iEXO-OXA on primary pancreatic tumor-bearing mice

Inspired by the above *in vitro* results, we further assessed the therapeutic capability of various formulations in orthotopic pancreatic tumor-bearing C57BL/6 mice. After the implantation of luciferase stable-transfected PANC-02 cell lines in the pancreas, the mouse models were randomly divided into seven groups and injected with phosphate buffer saline (group PBS), gemcitabine (group GEM), oxaliplatin (group OXA), scrambled siRNA-loaded exosomes (group Scrbl-iEXO), gal-9 siRNA-loaded exosomes (group iEXO), OXA prodrug-modified exosomes (group EXO-OXA), and gal-9 siRNA and OXA codelivery exosomes (group iEXO-OXA) every 3 days for 5 times (Fig. 4a). The combined immunotherapy, iEXO-OXA, resulted in robust anti-tumor effects, leading to a remarkable reduction in tumor size (Fig. 4b) and tumoral bioluminescence ($*P < 0.05$, Fig. 4c and f), as well as the longest life span (Fig. 4d and Fig. S13), better than the treatment of gemcitabine, the standard drug for PDAC. In contrast, mice received iEXO or EXO-OXA

alone failed to inhibit the tumor growth in this model. Moreover, there was no evident weight loss or organ toxicity throughout the whole studies showing the biosafety of our exosome-based formulations *in vivo* (Fig. 4e and Fig. S19).

To explore the mechanisms underlying the satisfactory antitumor efficacy of iEXO-OXA, multiple elements within the tumor site were investigated. Firstly, macrophage polarization to tumor-suppressive M1 phenotype was achieved through iEXO or iEXO-OXA treatment because of the down regulation of galectin-9 in the tumor cells (Fig. 5a–d, g–h). The reduced population of M2-TAMs ($CD45^+CD11b^+CD206^+$) as well as increased M1-TAMs ($CD45^+CD11b^+CD16/32^+$) were observed in group iEXO and iEXO-OXA by FACS and immunofluorescence staining of the tumor sections. These changes were considered as improvement of the immunosuppressive TME. Notably, other studies also found robust expression of galectin-9 in both tumor site and serum of PDAC patients, showing the potential of galectin-9 as a new biomarker for detection of PDAC [9]. Besides, it has been reported that galectin-9 is highly expressed in several other tumors with different influence. Whereas increased expression was related to decreased survival in lung adenocarcinoma, high expression was associated with antimetastatic potential in breast cancer and lower survival in cancers like hepatocellular carcinoma, gastric cancer and colon cancer [39–43]. These findings suggest the potential use of the demonstrated formulation in other cancers.

Secondly, compared with group PBS, GEM and Scrbl-iEXO, increased

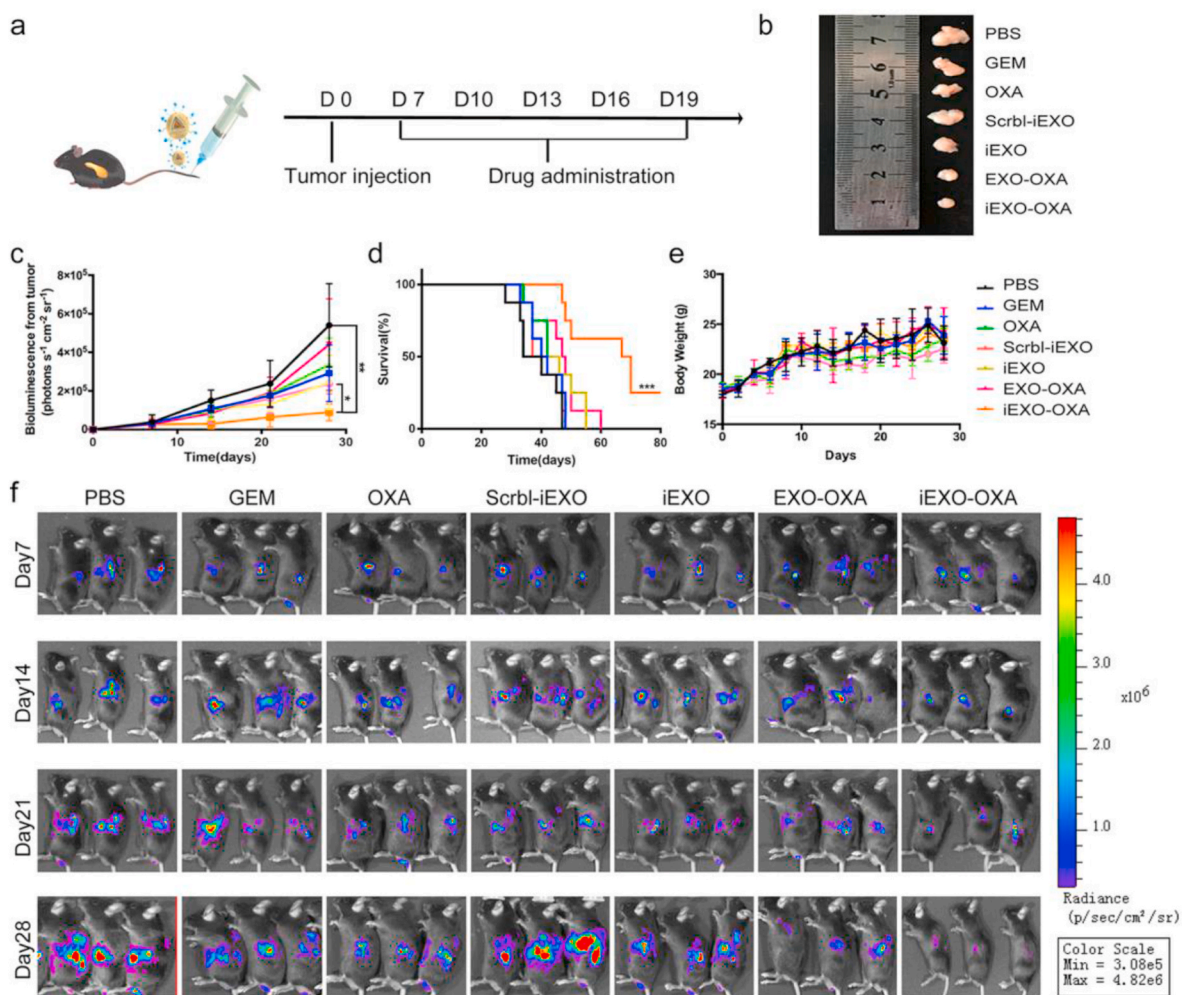


Fig. 4. *In vivo* antitumor efficacy of iEXO-OXA. a) Time schedule of drug treatment. b) Tumor size, c) statistic bioluminescence, d) survival rate, and e) body weight of the mice during the 4-week treatment course ($n = 8$, *i.v.*, 5 mg OXA/kg, $\sim 10^8$ exosomes per mouse). f) Real-time *in vivo* bioluminescence images at day 7, 14, 21, 28 by IVIS. Mice were treated with different formulations at day 7, 10, 13, 16, 19 ($n = 8$). Data presented as means \pm SD, one-way ANOVA, $*p < 0.05$, $**p < 0.01$, $***p < 0.001$.

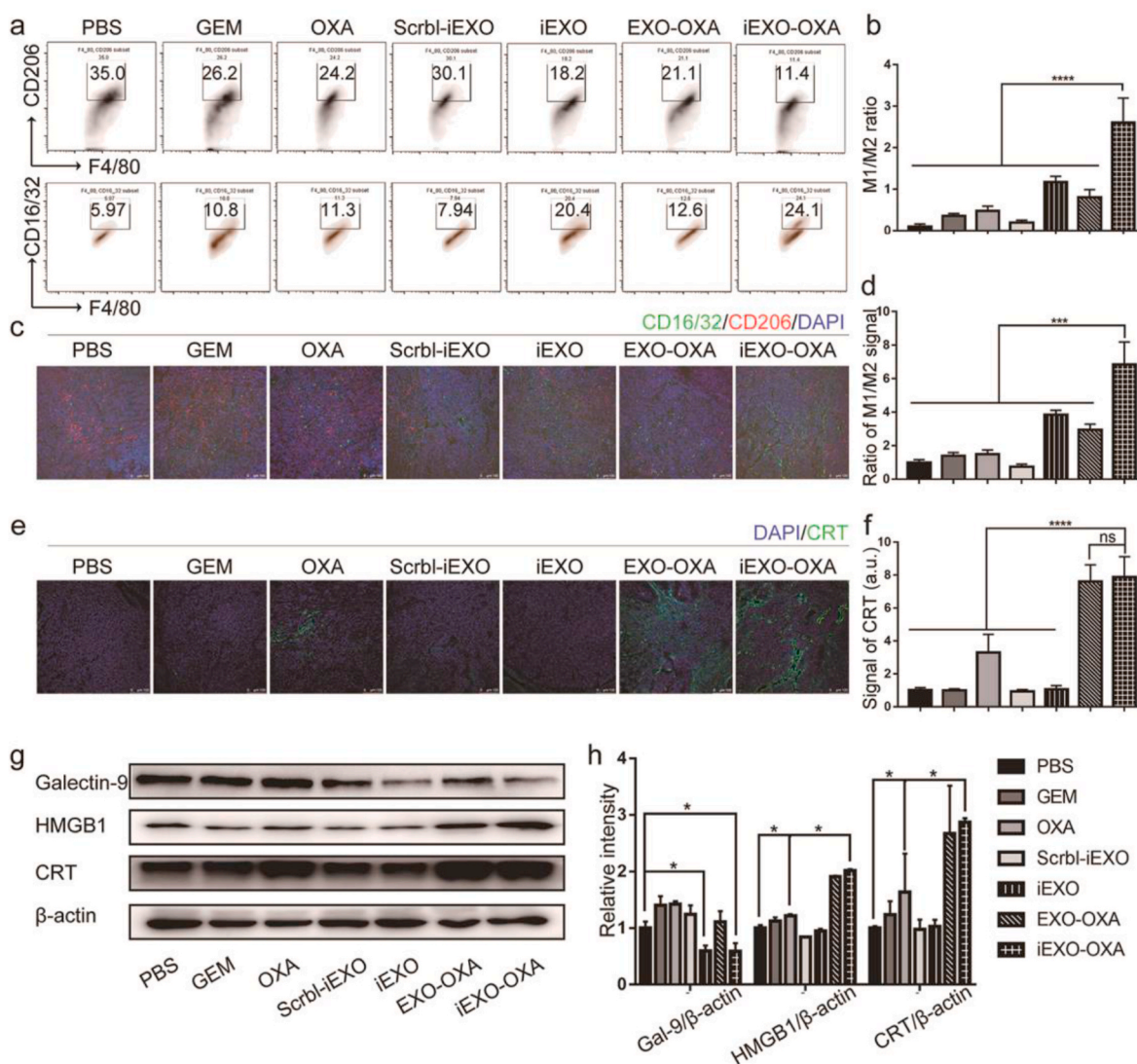


Fig. 5. Enhanced ICD and macrophage polarization of iEXO-OXA *in vivo*. a) iEXO-OXA increased macrophage polarization from M2-like phenotype (CD206 marker) to M1-like phenotype (CD16/32 marker). b) Statistical results of M1/M2 ratio ($n = 3$). c) Immunostaining of CD16/32 (M1 marker) and CD206 (M2 marker) to determine macrophage phenotype in treatment with different formulations (green: CD16/32; red: CD206; blue: DAPI; scale bar: 100 μ m). d) Statistical results of c) ($n = 3$). e) Immunostaining of CRT exposure after treatment with different formulations in tumor tissues (green: CRT; blue: DAPI; scale bar: 100 μ m). f) Statistical results of e) ($n = 3$). g) Western blotting of galectin-9 expression and HMGB1 release in tumor tissues. h) Statistical results of g) ($n = 3$). Data presented as means \pm SD, one-way ANOVA, * $p < 0.05$, ** $p < 0.001$, **** $p < 0.0001$.

ICD responses were found in the tumor region in group OXA as higher level of CRT exposure and HMGB1 release were confirmed by CLSM and western blotting, although not as prominent as group EXO-OXA (Fig. 5e–h). As the consequence, these up-regulated immunostimulatory “danger” signals promoted more population of mature DCs in group EXO-OXA (Fig. 6a and b). It has been reported that DCs play a crucial role in boosting immune response in tumor draining lymph nodes (TDLN) and infiltration of intratumoral CD8⁺ CTLs [44]. Therefore, treatment with EXO-OXA resulted in higher ratio of cytotoxic T cells and helper T cells confirmed by FACS and immunofluorescent staining (Fig. 6c–d, g–h). In turn, lower percentage of regulatory T cells were detected in these groups (Fig. 6e–f, i–j). When investigating iEXO-OXA treated mice models, we found that the combined treatment resulted in the most abundant population of CD8⁺ CTLs and the lowest ratio of Tregs, demonstrating that the dual delivery biosystem synergistically enhanced antitumor effect compared to other treatments. The elevated level of interferon- γ (IFN- γ) and decreased level of interleukin-10 (IL-10) in the tumor site of group iEXO-OXA further verified the conclusion (Fig. S20).

Notably, from images of immunofluorescence staining of the tumor sections in Fig. 6k, we could see that pancreatic cancer nests looked like islands in the stroma in group PBS. Although treated with chemotherapeutics (group GEM and OXA) or gene drugs (iEXO), increased (but not so significant) immune cells like CD8⁺ CTLs were still trapped in the extracellular matrix (CD8⁺ CTLs were co-localized with COL-1) and hardly observed in the deeper site of tumor nests. This explained why these groups could not achieve satisfactory antitumor efficacy. In contrast, when we delivered ICD indicator OXA with siRNA treatment (group iEXO-OXA) to reverse immunosuppressive TME, remarkable immune cells were infiltrated into the tumor nests instead of just co-localizing with stroma. Taken together, we substantiated that the combined immunotherapy could produce a synergetic effect and influence the cellular crosstalk *in vivo*, leading to an overall change of TME, thus enhancing the antitumor efficacy.

4. Conclusion

In conclusion, we demonstrated an exosome-based dual delivery

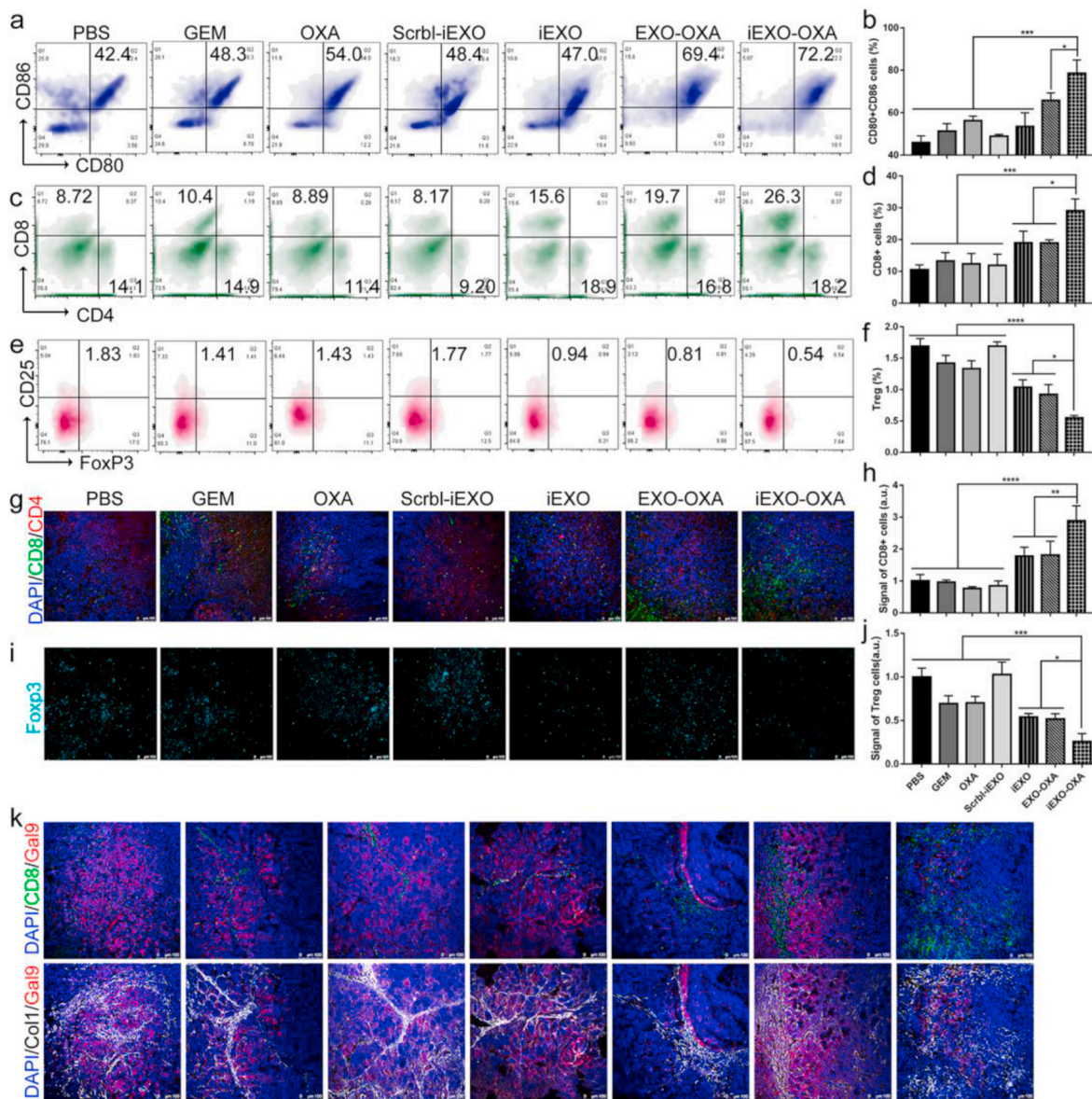


Fig. 6. Enhanced immunity of iEXO-OXA. Representative plots of a) mature DCs, c) CD8⁺T cells and CD4⁺T cells, and e) Treg cells in orthotopic PANC-02 tumor-bearing mice after various treatments analyzed by flow cytometry. b), d) and f) Statistical results of a), c) and e), respectively (n = 3). g) Immunofluorescence of CD8 and CD4 in tumor sections after different treatments (green: CD8; red: CD4; blue: DAPI; scale bar: 100 μ m). f) Statistical results of positive CD8 signaling in tumor sections (n = 3). g) Immunofluorescence of Foxp3 (representing Treg cells) in tumor sections after different treatments (blue: Foxp3; scale bar: 100 μ m). h) Statistical results of positive Foxp3 signaling in tumor sections (n = 3). f) Immunofluorescence of co-localization of CD8 (representing immune cells) and COL-1 (representing extracellular matrix) in tumor sections after different treatments (green: CD8; red: galectin-9; gray: collagen I; blue: DAPI; scale bar: 100 μ m). Data presented as means \pm SD, one-way ANOVA, * p < 0.05, ** p < 0.01, *** p < 0.001, **** p < 0.0001.

biosystem for accomplishing synergistic immune response in orthotopic PDAC mice through induction of ICD stimulus as well as interfering in immune suppression. The tumor-homing ability of the biocarriers, exosomes further endowed drug accumulation in tumor regions while decreased the systemic distribution to avoid side effect. The combined formulation iEXO-OXA induced effective innate and adaptive anti-PDAC immunity through enhanced ICD induction, improved DC maturation, reversed immunosuppression and increased infiltration of antitumoral cytotoxic T lymphocytes.

Credit author statement

Wenxi Zhou: Conceptualization, Methodology, Software, Validation, Formal analysis, Investigation, Data curation, Writing – original draft, Visualization. Yu Zhou: Methodology, Validation. Xinli Chen:

Methodology, Software, Validation. Tingting Ning: Methodology, Validation. Hongyi Chen: Formal analysis, Investigation. Qin Guo: Formal analysis, Investigation. Yiwen Zhang: Formal analysis, Investigation. Peixin Liu: Investigation, Data curation. Yujie Zhang: Investigation, Data curation. Chao Li: Investigation. Yongchao Chu: Investigation. Tao Sun: Conceptualization, Methodology, Writing – review & editing, Supervision. Chen Jiang: Conceptualization, Methodology, Resources, Writing – review & editing, Supervision, Project administration, Funding acquisition.

Declaration of competing interest

The authors declare that they have no known competing financial interests or personal relationships that could have appeared to influence the work reported in this paper.

Acknowledgments

We acknowledge Prof. Zhigang Zhang at Shanghai Cancer Institute for providing the PANC02 cell lines. We also acknowledge the support from the National Natural Science Foundation of China (grant No. 32030059), Program of Shanghai Academic Research Leader (18XD1400500), Key projects of Shanghai Science Foundation (19JC1410800) and Shanghai Municipal Science and Technology Major Project (No.2018SHZDZX01) and ZJLab.Data and materials availability: All data needed to support the conclusions are present in the paper and/or the Supplementary Materials. Additional data related to this paper may be requested from the authors.

Appendix A. Supplementary data

Supplementary data to this article can be found online at <https://doi.org/10.1016/j.biomaterials.2020.120546>.

References

- [1] D.P. Ryan, T.S. Hong, N. Bardeesy, Pancreatic adenocarcinoma, *N. Engl. J. Med.* 371 (11) (2014) 1039–1049.
- [2] C. Feig, J.O. Jones, M. Kraman, R.J. Wells, A. Deonarine, D.S. Chan, C.M. Connell, E.W. Roberts, Q. Zhao, O.L. Caballero, S.A. Teichmann, T. Janowitz, D.I. Jodrell, D. A. Tuveson, D.T. Fearon, Targeting CXCL12 from FAP-expressing carcinoma-associated fibroblasts synergizes with anti-PD-L1 immunotherapy in pancreatic cancer, *Proc. Natl. Acad. Sci. U. S. A.* 110 (50) (2013) 20212–20217.
- [3] S.L. Topalian, C.G. Drake, D.M. Pardoll, Immune checkpoint blockade: a common denominator approach to cancer therapy, *Canc. Cell* 27 (4) (2015) 450–461.
- [4] P.C. Tumeh, C.L. Harview, J.H. Yearley, I.P. Shintaku, E.J. Taylor, L. Robert, B. Chmielowski, M. Spasic, G. Henry, V. Ciobanu, A.N. West, M. Carmona, C. Kivork, E. Seja, G. Cherry, A.J. Gutierrez, T.R. Grogan, C. Mateus, G. Tomasic, J. A. Glaspy, R.O. Emerson, H. Robins, R.H. Pierce, D.A. Elashoff, C. Robert, A. Ribas, PD-1 blockade induces responses by inhibiting adaptive immune resistance, *Nature* 515 (7528) (2014) 568–571.
- [5] C.E. Clark, S.R. Hingorani, R. Mick, C. Combs, D.A. Tuveson, R.H. Vonderheide, Dynamics of the immune reaction to pancreatic cancer from inception to invasion, *Canc. Res.* 67 (19) (2007) 9518–9527.
- [6] J.Q. Fan, M.F. Wang, H.L. Chen, D. Shang, J.K. Das, J. Song, Current advances and outlooks in immunotherapy for pancreatic ductal adenocarcinoma, *Mol. Canc.* 19 (1) (2020) 32.
- [7] A.H. Morrison, K.T. Byrne, R.H. Vonderheide, Immunotherapy and prevention of pancreatic cancer, *Trends Cancer* 4 (6) (2018) 418–428.
- [8] D. Daley, V.R. Mani, N. Mohan, N. Akkad, A. Ochi, D.W. Heindel, K.B. Lee, C. P. Zambirinis, G.S.B. Pandian, S. Savadkar, A. Torres-Hernandez, S. Nayak, D. Wang, M. Hundeyin, B. Diskin, B. Aykut, G. Werba, R.M. Barilla, R. Rodriguez, S. Chang, L. Gardner, L.K. Mahal, B. Ueberheide, G. Miller, Dectin 1 activation on macrophages by galectin 9 promotes pancreatic carcinoma and peritumoral immune tolerance, *Nat. Med.* 23 (5) (2017) 556–567.
- [9] A.M. Seifert, C. Reiche, M. Heiduk, A. Tannert, A.C. Meinecke, S. Baier, J. von Renesse, C. Kahlert, M. Distler, T. Welsch, C. Reissfelder, D.E. Aust, G. Miller, J. Weitz, L. Seifert, Detection of pancreatic ductal adenocarcinoma with galectin-9 serum levels, *Oncogene* 39 (15) (2020) 3102–3113.
- [10] R.W. Cowan, A. Maitra, Genetic progression of pancreatic cancer, *Canc. J.* 20 (1) (2014) 80–84.
- [11] A.A. Rucki, L. Zheng, Pancreatic cancer stroma: understanding biology leads to new therapeutic strategies, *World J. Gastroenterol.* 20 (9) (2014) 2237–2246.
- [12] O.S. Fenton, K.N. Olafson, P.S. Pillai, M.J. Mitchell, R. Langer, Advances in biomaterials for drug delivery, *Adv. Mater.* (2018), e1705328.
- [13] A. Wang-Gillam, R.A. Hubner, J.T. Siveke, D.D. Von Hoff, B. Belanger, F.A. de Jong, B. Mirakhor, L.T. Chen, NAPOLI-1 phase 3 study of liposomal irinotecan in metastatic pancreatic cancer: final overall survival analysis and characteristics of long-term survivors, *Eur. J. Canc.* 108 (2019) 78–87.
- [14] J.M. Stewart, B.G. Keselowsky, Combinatorial drug delivery approaches for immunomodulation, *Adv. Drug Deliv. Rev.* 114 (2017) 161–174.
- [15] M.S. Kim, M.J. Haney, Y. Zhao, Y. Mahajan, I. Deygen, N.L. Klyachko, E. Inskoe, A. Piroyan, M. Sokolsky, O. Okolie, S.D. Hingtgen, A.V. Kabanov, E.V. Batrakov, Development of exosome-encapsulated paclitaxel to overcome MDR in cancer cells, *Nanomedicine* 12 (3) (2016) 655–664.
- [16] P. Vader, E.A. Mol, G. Pasterkamp, R.M. Schiffelers, Extracellular vesicles for drug delivery, *Adv. Drug Deliv. Rev.* 106 (Pt A) (2016) 148–156.
- [17] T.H. Tran, G. Mattheolabakis, H. Aldawsari, M. Amiji, Exosomes as nanocarriers for immunotherapy of cancer and inflammatory diseases, *Clin. Immunol.* 160 (1) (2015) 46–58.
- [18] Y. Zhou, W. Zhou, X. Chen, Q. Wang, C. Li, Q. Chen, Y. Zhang, Y. Lu, X. Ding, C. Jiang, Bone marrow mesenchymal stem cells-derived exosomes for penetrating and targeted chemotherapy of pancreatic cancer, *Acta Pharm. Sin. B* 10 (8) (2019) 1563–1575.
- [19] R.H. Vonderheide, L.J. Bayne, Inflammatory networks and immune surveillance of pancreatic carcinoma, *Curr. Opin. Immunol.* 25 (2) (2013) 200–205.
- [20] J. Lu, X. Liu, Y.P. Liao, F. Salazar, B. Sun, W. Jiang, C.H. Chang, J. Jiang, X. Wang, A.M. Wu, H. Meng, A.E. Nel, Nano-enabled pancreas cancer immunotherapy using immunogenic cell death and reversing immunosuppression, *Nat. Commun.* 8 (1) (2017) 1811.
- [21] M. Obeid, A. Tesniere, F. Ghiringhelli, G.M. Fimia, L. Apetoh, J.L. Perfettini, M. Castedo, G. Mignot, T. Panaretakis, N. Casares, D. Metivier, N. Larochette, P. van Endert, F. Ciccosanti, M. Piacentini, L. Zitvogel, G. Kroemer, Calreticulin exposure dictates the immunogenicity of cancer cell death, *Nat. Med.* 13 (1) (2007) 54–61.
- [22] M. Michaud, I. Martins, A.Q. Sukkurwala, S. Adjemian, Y. Ma, P. Pellegatti, S. Shen, O. Kepp, M. Scoazec, G. Mignot, S. Rello-Varona, M. Tailler, L. Menger, E. Vacchelli, L. Galluzzi, F. Ghiringhelli, F. Di Virgilio, L. Zitvogel, G. Kroemer, Autophagy-dependent anticancer immune responses induced by chemotherapeutic agents in mice, *Science* 334 (6062) (2011) 1573–1577.
- [23] L. Apetoh, F. Ghiringhelli, A. Tesniere, M. Obeid, C. Ortiz, A. Criollo, G. Mignot, M. C. Maiuri, E. Ullrich, P. Saulnier, H. Yang, S. Amigorena, B. Ryffel, F.J. Barrat, P. Saftig, F. Levi, R. Lidereau, C. Nogues, J.P. Mira, A. Chompret, V. Joulin, F. Clavel-Chapelon, J. Bourhis, F. Andre, S. Delaloge, T. Tursz, G. Kroemer, L. Zitvogel, Toll-like receptor 4-dependent contribution of the immune system to anticancer chemotherapy and radiotherapy, *Nat. Med.* 13 (9) (2007) 1050–1059.
- [24] L. Liu, Q. Chen, C. Ruan, X. Chen, Y. Zhang, X. He, Y. Zhang, Y. Lu, Q. Guo, T. Sun, H. Wang, C. Jiang, Platinum-based nanovectors engineered with immunomodulating adjuvant for inhibiting tumor growth and promoting immunity, *Theranostics* 8 (11) (2018) 2974–2987.
- [25] B. Feng, F. Zhou, B. Hou, D. Wang, T. Wang, Y. Fu, Y. Ma, H. Yu, Y. Li, Binary cooperative prodrug nanoparticles improve immunotherapy by synergistically modulating immune tumor microenvironment, *Adv. Mater.* 30 (38) (2018), e1803001.
- [26] S. Kamerkar, V.S. LeBleu, H. Sugimoto, S. Yang, C.F. Ruivo, S.A. Melo, J.J. Lee, R. Kalluri, Exosomes facilitate therapeutic targeting of oncogenic KRAS in pancreatic cancer, *Nature* 546 (7659) (2017) 498–503.
- [27] W. Huang, X. Wu, X. Gao, Y. Yu, H. Lei, Z. Zhu, Y. Shi, Y. Chen, M. Qin, W. Wang, Y. Cao, Maleimide-thiol adducts stabilized through stretching, *Nat. Chem.* 11 (4) (2019) 310–319.
- [28] V. Baron-Bodo, P. Doceur, M.L. Lefebvre, K. Labroquere, C. Defaye, C. Cambouris, D. Prigent, M. Salcedo, A. Boyer, A. Nardin, Anti-tumor properties of human-activated macrophages produced in large scale for clinical application, *Immunobiology* 210 (2–4) (2005) 267–277.
- [29] L. Alvarez-Erviti, Y. Seow, H. Yin, C. Betts, S. Lakkhal, M.J. Wood, Delivery of siRNA to the mouse brain by systemic injection of targeted exosomes, *Nat. Biotechnol.* 29 (4) (2011) 341–345.
- [30] S. El-Andaloussi, Y. Lee, S. Lakkhal-Littleton, J. Li, Y. Seow, C. Gardiner, L. Alvarez-Erviti, I.L. Sargent, M.J. Wood, Exosome-mediated delivery of siRNA in vitro and in vivo, *Nat. Protoc.* 7 (12) (2012) 2112–2126.
- [31] L.A. Mulcahy, R.C. Pink, D.R. Carter, Routes and mechanisms of extracellular vesicle uptake, *J. Extracell. Vesicles* 3 (2014).
- [32] H. Costa Verdera, J.J. Gitz-Francois, R.M. Schiffelers, P. Vader, Cellular uptake of extracellular vesicles is mediated by clathrin-independent endocytosis and macropinocytosis, *J. Contr. Release* 266 (2017) 100–108.
- [33] S. Horibe, T. Tanahashi, S. Kawauchi, Y. Murakami, Y. Rikitake, Mechanism of recipient cell-dependent differences in exosome uptake, *BMC Canc.* 18 (1) (2018) 47.
- [34] A. Kabashima-Niibe, H. Higuchi, H. Takaishi, Y. Masugi, Y. Matsuzaki, Y. Mabuchi, S. Funakoshi, M. Adachi, Y. Hamamoto, S. Kawachi, K. Aiura, Y. Kitagawa, M. Sakamoto, T. Hibi, Mesenchymal stem cells regulate epithelial-mesenchymal transition and tumor progression of pancreatic cancer cells, *Canc. Sci.* 104 (2) (2013) 157–164.
- [35] S. Wen, M. Dooner, Y. Cheng, E. Papa, M. Del Totto, M. Pereira, Y. Deng, L. Goldberg, J. Aliotta, D. Chatterjee, C. Stewart, A. Carpanetto, F. Collino, S. Bruno, G. Camussi, P. Quesenberry, Mesenchymal stromal cell-derived extracellular vesicles rescue radiation damage to murine marrow hematopoietic cells, *Leukemia* 30 (11) (2016) 2221–2231.
- [36] O.P. Wiklander, J.Z. Nordin, A. O'Loughlin, Y. Gustafsson, G. Corso, I. Mager, P. Vader, Y. Lee, H. Sork, Y. Seow, N. Heldring, L. Alvarez-Erviti, C.I. Smith, K. Le Blanc, P. Macchiarini, P. Jungebluth, M.J. Wood, S.E. Andaloussi, Extracellular vesicle in vivo biodistribution is determined by cell source, route of administration and targeting, *J. Extracell. Vesicles* 4 (2015) 26316.
- [37] R.W. Yeo, R.C. Lai, B. Zhang, S.S. Tan, Y. Yin, B.J. Teh, S.K. Lim, Mesenchymal stem cell: an efficient mass producer of exosomes for drug delivery, *Adv. Drug Deliv. Rev.* 65 (3) (2013) 336–341.
- [38] G. Kroemer, L. Galluzzi, O. Kepp, L. Zitvogel, Immunogenic cell death in cancer therapy, *Annu. Rev. Immunol.* 31 (2013) 51–72.
- [39] K. Sideras, K. Biermann, J. Verheij, B.R. Takkenberg, S. Mancham, B.E. Hansen, H. M. Schutz, R.A. de Man, D. Sprengers, S.I. Buschow, M.C. Versepoot, P.P. Boor, Q. Pan, T.M. van Gulik, T. Terkivatan, J.N. Ijzermans, U.H. Beuers, S. Sleijfer, M. J. Bruno, J. Kwekkeboom, PD-L1, Galectin-9 and CD8+ tumor-infiltrating lymphocytes are associated with survival in hepatocellular carcinoma, *Oncolimmunology* 6 (2) (2017), e1273309.
- [40] J. Jiang, M.S. Jin, F. Kong, D. Cao, H.X. Ma, Z. Jia, Y.P. Wang, J. Suo, X. Cao, Decreased galectin-9 and increased Tim-3 expression are related to poor prognosis in gastric cancer, *PLoS One* 8 (12) (2013), e81799.
- [41] Y. Wang, J. Sun, C. Ma, W. Gao, B. Song, H. Xue, W. Chen, X. Chen, Y. Zhang, Q. Shao, Q. Wang, L. Zhao, J. Liu, X. Wang, H. Wang, Y. Zhang, M. Yang, X. Qu, Reduced expression of galectin-9 contributes to a poor outcome in colon cancer by inhibiting NK cell chemotaxis partially through the rho/ROCK1 signaling pathway, *PLoS One* 11 (3) (2016), e0152599.

- [42] Y. Ohue, K. Kurose, R. Nozawa, M. Isobe, Y. Nishio, T. Tanaka, Y. Doki, T. Hori, J. Fukuoka, M. Oka, E. Nakayama, Survival of lung adenocarcinoma patients predicted from expression of PD-L1, galectin-9, and XAGE1 (GAGED2a) on tumor cells and tumor-infiltrating T cells, *cancer immunol. Res.* 4 (12) (2016) 1049–1060.
- [43] A. Irie, A. Yamauchi, K. Kontani, M. Kihara, D. Liu, Y. Shirato, M. Seki, N. Nishi, T. Nakamura, H. Yokomise, M. Hirashima, Galectin-9 as a prognostic factor with antimetastatic potential in breast cancer, *Clin. Canc. Res.* 11 (8) (2005) 2962–2968.
- [44] O.P. Joffre, E. Segura, A. Savina, S. Amigorena, Cross-presentation by dendritic cells, *Nat. Rev. Immunol.* 12 (8) (2012) 557–569.